Earth and Planetary Science Letters 432 (2015) 133–141

Contents lists available at ScienceDirect

Earth and Planetary Science Letters

www.elsevier.com/locate/epsl

Accurate focal depth determination of oceanic earthquakes using water-column reverberation and some implications for the shrinking plate hypothesis

Jianping Huang [a,b], Fenglin Niu [b,c,*], Richard G. Gordon [b], Chao Cui [a]

[a] Department of Geosciences, China University of Petroleum, Qingdao, Shandong, 266580, China
[b] Department of Earth Science, Rice University, Houston, TX, 77005, USA
[c] State Key Laboratory of Petroleum Resources and Prospecting, and Unconventional Natural Gas Institute, China University of Petroleum, Beijing, 102249, China

ARTICLE INFO

Article history:
Received 28 July 2015
Received in revised form 30 September 2015
Accepted 1 October 2015
Available online 3 November 2015
Editor: P. Shearer

Keywords:
focal depth
oceanic earthquakes
water-column reverberations
Z–H grid search
oceanic lithosphere cooling model
horizontal contraction of oceanic plates

ABSTRACT

Investigation of oceanic earthquakes is useful for constraining the lateral and depth variations of the stress and strain-rate fields in oceanic lithosphere, and the thickness of the seismogenic layer as a function of lithosphere age, thereby providing us with critical insight into thermal and dynamic processes associated with the cooling and evolution of oceanic lithosphere. With the goal of estimating hypocentral depths more accurately, we observe clear water reverberations after the direct P wave on teleseismic records of oceanic earthquakes and develop a technique to estimate earthquake depths by using these reverberations. The Z–H grid search method allows the simultaneous determination of the sea floor depth (H) and earthquake depth (Z) with an uncertainty less than 1 km, which compares favorably with alternative approaches. We apply this method to two closely located earthquakes beneath the eastern Pacific. These earthquakes occurred in ∼25 Ma-old lithosphere and were previously estimated to have similar depths of ∼10–12 km. We find that the two events actually occurred at dissimilar depths of 2.5 km and 16.8 km beneath the seafloor, respectively, within the oceanic crust and lithospheric mantle. The shallow and deep events are determined to be a thrust and normal earthquake, respectively, indicating that the stress field within the oceanic lithosphere changes from horizontal deviatoric compression to horizontal deviatoric tension as depth increases, which is consistent with the prediction of lithospheric cooling models. Furthermore, we show that the P-axis of the newly investigated thrust-faulting earthquake is perpendicular to that of the previously studied thrust event, consistent with the predictions of the shrinking-plate hypothesis.

1. Introduction

Depth estimates of oceanic earthquakes have been useful in the investigation of many problems of tectonophysics: depth extent of the seismogenic layer in intraplate settings (Okal et al., 1980; Bergman and Solomon, 1980; Wiens and Stein, 1983) and the corresponding limiting temperature above which earthquakes do not nucleate (McKenzie et al., 2005), along mid-ocean ridges (Huang and Solomon, 1988), along transform faults (Engeln et al., 1986; Bergman and Solomon, 1988), and along the outer rise of trenches.

Source mechanisms of intraplate oceanic earthquakes have been used to infer the state of stress of the lithosphere (e.g., Sykes and Sbar, 1974; Stein and Okal, 1978; Wiens and Stein, 1983; Bergman and Solomon, 1984; Zoback et al., 1989). Sykes and Sbar (1974) studied focal mechanism solutions of earthquakes occurring off the mid-ocean ridge axis using P-wave first motion data, and found that most earthquakes occurring in oceanic lithosphere older than ∼15 Ma indicate thrust faulting while those observed in the younger oceanic lithosphere indicate normal faulting. This change in focal mechanism was interpreted as a stress state transition from ridge axis (horizontal deviatoric tensional) to intraplate stress (horizontal deviatoric compressional) regime. Wiens and Stein (1984), however, found mixed types of earthquake mechanisms occurring in oceanic lithosphere between 3 and 35 Ma and concluded that there is a no general tensional-to-compressive stress transition in the oceanic lithosphere. On the other hand, different types of earthquake mechanisms observed for the same lithospheric age have different focal depth (Bergman and Solomon, 1984; Wiens and Stein, 1984), indicating that there is a stress state change with depth. These are now interpreted as

* Corresponding author at: Department of Earth Science, Rice University, Houston, TX, 77005, USA. Tel.: +1 713 348 4122.
E-mail address: niu@rice.edu (F. Niu).

http://dx.doi.org/10.1016/j.epsl.2015.10.001
0012-821X/

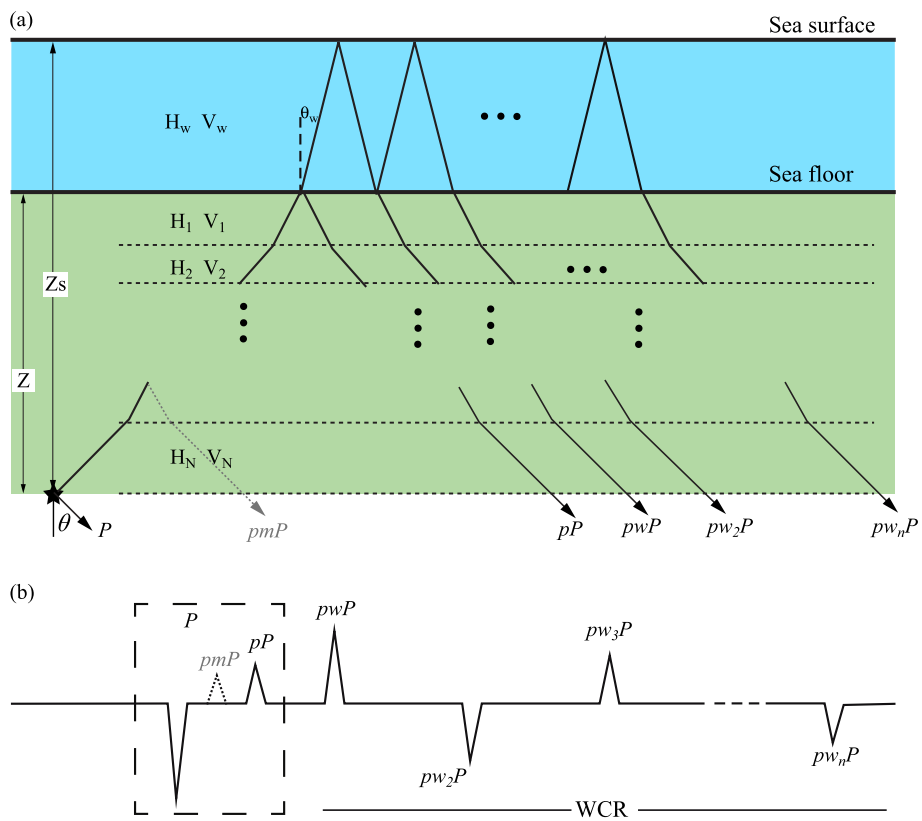

Fig. 1. (a) A schematic diagram showing the ray paths of the P, pP, pwP, and the water reverberations pw_nP. The upper and lower layers shaded with light blue and green indicate the seawater and oceanic lithosphere, respectively. The horizontal dashed lines represent the boundaries of constant velocity layers in the reference velocity model with a thickness of H_i and velocity V_i. (b) A schematic seismogram showing the sequence of arrivals in a vertical record of an oceanic earthquake at teleseismic distances. (For interpretation of the references to color in this figure legend, the reader is referred to the web version of this article.)

being due to depth-dependent stress and strain. Numerical modeling also suggests that the stress field within the lithosphere varies systematically and significantly with depth. The upper and the lower competent lithosphere are in horizontal deviatoric compression and tension, respectively (Parmentier and Haxby, 1986; Wessel, 1992). These investigations have helped to establish the role of thermo-elastic stresses in the evolution of oceanic lithosphere (Parmentier and Haxby, 1986; Wessel, 1992)

Recently, source mechanisms of oceanic intraplate earthquakes and their depth dependence have come under renewed interest because of the hypothesis that horizontal thermal contraction of the lithosphere may lead to measurable non-rigidity of oceanic plates (Kumar and Gordon, 2009; Kreemer and Gordon, 2014; Mishra and Gordon, submitted for publication). Kumar and Gordon (2009) estimate that vertically averaged strain rates due to thermal contraction vary as $\sim t^{-1}$, where t is the age of the lithosphere, with vertically averaged horizontal contraction rates ranging from 10^{-5} Ma^{-1} (3×10^{-19} s^{-1}) to 2×10^{-2} Ma^{-1} (5×10^{-16} s^{-1}) (Kumar and Gordon, 2009; Mishra and Gordon, submitted for publication). Such strain rates accumulated across the Pacific plate may sum to significant displacement rates ($\sim$2 mm a^{-1}), which are non-negligible in estimating global plate velocity (Kumar and Gordon, 2009; Kreemer and Gordon, 2014). This has caused renewed interest in the deformation of oceanic lithosphere, including that manifested in earthquakes. Because of the expected depth dependence of earthquake mechanisms, one cannot simply look at the epicenters associated with focal mechanisms or centroid-moment tensors—one must also know the depth of the event. It is therefore appropriate to seek methods to obtain more accurate estimates of the depths of oceanic earthquakes, which are thought to have uncertainties of $\pm$1 km or more (Bergman and Solomon, 1984; Wiens and Stein, 1984).

The tradeoff between earthquake origin time and focal depth is a well known problem in hypocentral inversion. One of the most reliable ways of constraining focal depths is to identify the depth phases (pP and sP) and add their arrival times in the inversion. Many methods have been developed to improve the identification of depth phases in seismograms, from simple stacking technique using array data (e.g., Key, 1968) to more sophisticated techniques, such as the F-detector technique proposed by Heyburn and Browers (2008). The above routine depth-phase method, however, works only when the depth arrivals are located outside the source time window such that they can be robustly picked. Assuming a source time function of 5 s, the minimum source depth that can be constrained with the routine depth-phase method is $\sim$15 km. Chu et al. (2009) developed an iterative waveform fitting method to determine earthquake focal depths and source time functions using teleseismic P waves. This method, however, requires full knowledge of the moment tensor solutions of earthquakes, which could be difficult to obtain for intermediate-size earthquakes ($\sim$M5.0). It also becomes increasingly challenging to isolate the depth phases from the direct P wave since their ray parameters are nearly identical to the direct P wave when earthquakes occur at depths shallower than 5 km. The CAP (cut-and-paste) is another widely used method, which uses regional waveform data to search for the optimum focal mechanism and hypocentral depth (Zhao and Helmberger, 1994; Zhu and Helmberger, 1996). This method also requires a source time function, which is difficult to obtain when the direct P and the depth phases are mixed in the case of shallow earthquakes.

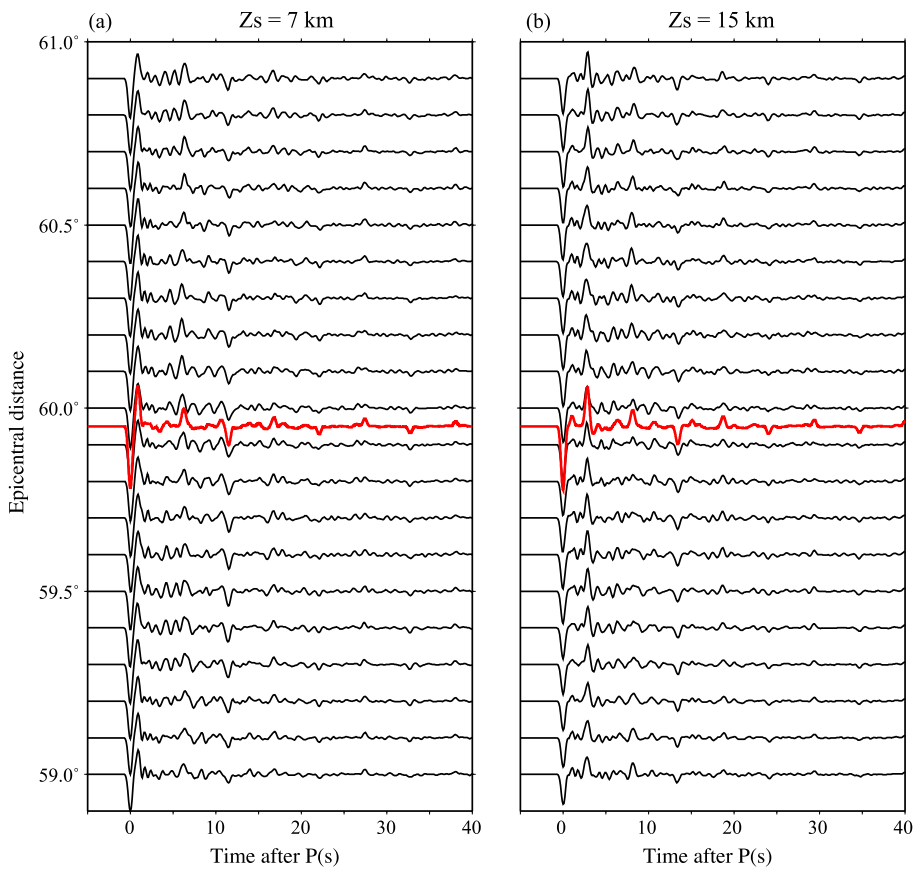

Fig. 2. The synthetic seismograms of an oceanic crust earthquake with a focal depth of 7 km and mantle earthquake at 15 km are plotted as a function of epicentral distance. The red traces shown in the middle are the sums of all the seismograms for each earthquake. A hybrid 1D velocity model, which has an oceanic crust in the source side and a continental crust in the receiver side (Table 1), is used in computing synthetics. (For interpretation of the references to color in this figure, the reader is referred to the web version of this article.)

Earthquake detection is challenging in the oceans due to the lack of local seismic stations, the presence of swell-generated noises, and high attenuation near the hypocentral region. From only P-wave arrival time data from teleseismic stations, the focal depth is in many cases poorly constrained. For example, Mendiguren (1971) studied an intraplate earthquake occurring on November 25, 1965 with an origin time of 10:50:40.2 and epicenter of 17.1°S and 100.2°W. The focal depth was estimated to be ∼45 km by USGS, and 143 ± 24 km by ISC.

The depth-phase series of oceanic earthquakes are more complicated because of the existence of the water column above the sea floor (Fig. 1a). As shown in Fig. 1, P-wave reflections at the sea floor (pP) and ocean surface (pwP) are expected to have a comparable amplitude. In addition to these two reflections, multiple reflections between sea floor and sea surface, which are referred to as $pw_{n+1}P$ $(n = 1, 2, \ldots)$ (Fig. 1b), are also expected to arrive periodically in time after the single reflections with alternately reversed polarity and decreasing amplitudes. Hereinafter we refer to all the sea surface reflections as water column reverberations (WCRs), including the single (pwP) and multiples $pw_{n+1}P$. These depth phases have been used to improve estimates of earthquake focal depths (e.g., Mendiguren, 1971; Okal et al., 1980; Stewart and Helmberger, 1981). For the earthquake mentioned above, Mendiguren (1971) was able to identify at least three clear arrivals after the direct P on several teleseismic recordings. If the second and third arrivals after P are assumed to be pP, then the corresponding focal depths would be approximately 40 and 70 km, respectively, which are inconsistent with the observed amplitudes of the Love and Rayleigh waves. By assuming the three later arrivals to be pP, pwP, and pw_2P, he obtained a focal depth of 13 km, which agrees with surface wave data. Another possibility, which was not discussed by Mendiguren (1971), is that the observed three later arrivals could be pwP, pw_2P, and pw_3P if the focus of the earthquake is shallow enough that the pP arrival is located within the P-wave time window.

Herein we systematically investigate the characteristics of the pP, sP, and pw_nP with synthetic data to determine whether the first later arrival is the pP, sP, or pwP phase. We then introduce a grid-search based algorithm to search for the optimal focal depth, Zs (measured from the water surface), and water layer thickness, H, by maximizing the summed amplitude of the WCRs after polarity corrections. Hereinafter we refer to this grid search technique as the Z–H analysis, where Z is the focal depth measured from the ocean floor. We apply Z–H analysis to two sets of synthetic seismograms computed with a hypocenter located inside the oceanic crust and upper mantle, respectively. We then employ the Z–H grid search method to relocate two oceanic earthquakes occurring east-southeast of the Tuamotu Archipelago on the Pacific plate with teleseismic data. We obtain focal depths that we expect to be more accurate than those obtained by other methods. The relocated focal depths differ significantly from routine estimates and provide new information on deformation and stress state in the Pacific plate. In particular, we show that normal faulting occurred 16.8 km beneath the seafloor, consistent with the mechanism and depth of a previously investigated nearby event. We furthermore show that a thrust event occurred in the crust, but with fault planes nearly orthogonal to a previously investigated nearby earthquake, an observation consistent with the shrinking plate hypothesis of Kumar and Gordon (2009).

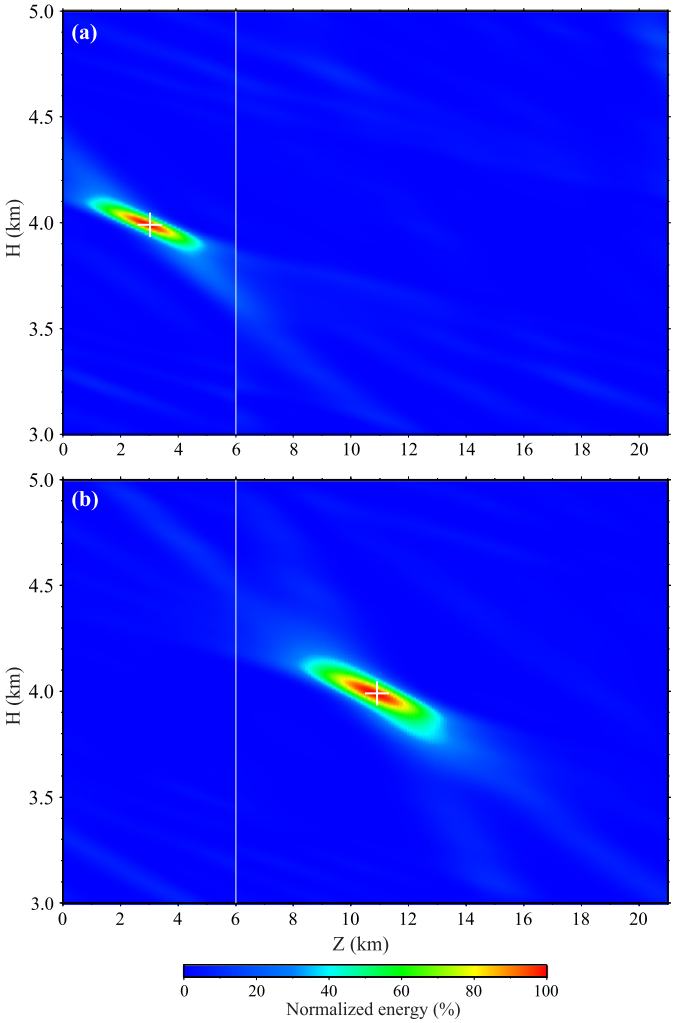

Fig. 3. The Z–H grid search results based on the synthetic seismograms of the 7 and 15 km deep earthquakes are shown respectively in (a) and (b). Color contour of summed amplitude as a function of earthquake depth below the sea floor (Z) and water layer thickness (H). Location of the amplitude peak is indicated by the white plus symbol. The thin vertical line indicates the Moho depth in kilometers measured from sea floor. The water layer thickness is 4 km in the synthetic model, thus the Moho depth is 6 km below the sea floor and 10 km below sea level. The estimated (Z, H) is (3.04, 3.99) km and (10.91, 4.00) km respectively for the 7-km and 15-km deep earthquakes. (For interpretation of the references to color in this figure legend, the reader is referred to the web version of this article.)

2. Method

2.1. Water-column reverberations

The P waveforms at teleseismic distances of 30° to 90° are known to be relatively simple due to the lack of triplications and diffraction associated with the upper-mantle discontinuities and the core–mantle boundary, respectively. Later arrivals associated with shallow oceanic earthquakes are thus relatively easy to identify from teleseismic records, especially after considering the characteristics of the WCRs featured by regular arrival times with alternating polarities. The ray paths of the WCRs are schematically shown in Fig. 1a. For shallow earthquakes, the ray parameters of the direct P, pP, and pw_nP are almost identical, which can be used to identify the origins of the later arrivals in addition to their arrival times and polarities. We identify the first WCR, *pwP*, from a teleseismic record by combining the above features on waveform polarity and arrival time.

As shown in the schematic synthetic seismogram in Fig. 1b, the later arrival sequence can consist of up to three arrivals (*pmP*, pP, and *pwP*) with similar polarity if the oceanic earthquake is deep enough. The first multiple (pw_2P) is then identified to be the next one showing an opposite polarity (Fig. 1c). Once the WCRs are identified, we use the grid search described below to find the optimum focal depth.

2.2. Z–H grid search

As shown in Fig. 1a, we first discretize the oceanic lithosphere in the source side by a stack of layers with constant P- and S-wave velocities. We assume that pP and WCRs travel with ray parameters identical to the direct P wave. In this case, the traveltime of pP and pw_nP relative to P can be written as:

$$\delta t_{pP} = 2\sum_{i=1}^{N} \frac{H_i \cos\theta_i}{\alpha_i}$$

$$\delta t_{pw_nP} = 2\sum_{i=1}^{N} \frac{H_i \cos\theta_i}{\alpha_i} + 2n\frac{H_w \cos\theta_w}{\alpha_w}, \quad (1)$$

where α_i, H_i, and θ_i are the P-wave velocity, layer thickness, and the incident angle in the ith layer with w indicating the water layer. The hypocenter is located at the bottom of the Nth layer, and thus the focal depth is $Z = \sum_{i=1}^{N} H_i$, measured from the seafloor.

We stack the first three WCRs, which usually have good signal-to-noise ratio (SNR), to search for the optimum focal depth, Z (measured from ocean floor), and water column thickness, H, that maximize the stacked amplitude given by the following equation:

$$S(Z,H) = \frac{C(Z,H)}{3\tau} \sum_{i=-\tau/2}^{\tau/2} \{d(t_{pwP} + i\Delta t) - d(t_{pw_2P} + i\Delta t) + d(t_{pw_3P} + i\Delta t)\}. \quad (2)$$

Here, $d(t)$ is the time sequence representing either an individual seismogram or a stacked trace of array records. Δt is the sampling interval, τ is the signal window length, and $C(Z,H)$ is the averaged cross correlation between pairs of the three WCRs after polarity correction. t_{pwP}, t_{pw2P}, and t_{pw3P} are the computed relative traveltimes of the first three WCRs corresponding to source and water depths, Z and H, respectively. Considering the negative polarity of the second reverberation, we assign a negative sign to it in the summation.

2.3. Synthetic tests

We generate synthetic waveforms using the modified Thomson–Haskell propagator matrix method developed by Wang (1999). The velocity model consists of an oceanic crust with a 4-km water layer over a 6-km crust in the source side, and a continental crust in the receiver side. The continental crust and mantle velocities are taken from the *iasp91* model (Kennett and Engdahl, 1991), while the velocities of the oceanic crust are listed in Table 1. We compute the synthetic seismograms for two earthquakes with focal depths of 7 and 15 km (below sea level), respectively, at distances between 59° and 60° with an increment of 0.1° (Figs. 2a and 2b). Given the Moho on the source side of 10 km below the sea level, they represent crustal and upper mantle earthquakes, respectively. We first align all the seismograms at the first trough of the P wave and then linearly stack all the synthetic seismograms to generate a high SNR teleseismic record (red traces in Fig. 2).

We then apply the Z–H grid search method using the stacked synthetic seismogram to search for the optimal focal depth (in the range of 0–21 km with an increment of 0.01 km) and sea floor

Table 1
Model parameters for the synthetic test.

Layer	Source side				Layer	Receiver side			
	Thickness (km)	V_p (km/s)	V_s (km/s)	Density (g/cm^3)		Thickness (km)	V_p (km/s)	V_s (km/s)	Density (g/cm^3)
Water	4.00	1.50	0.00	1.03	Upper crust	20.00	5.80	3.36	2.72
Crust	6.00	6.30	3.65	2.90	Lower crust	15.00	6.50	3.75	2.92
Mantle	iasp91 mantle					iasp91 mantle			

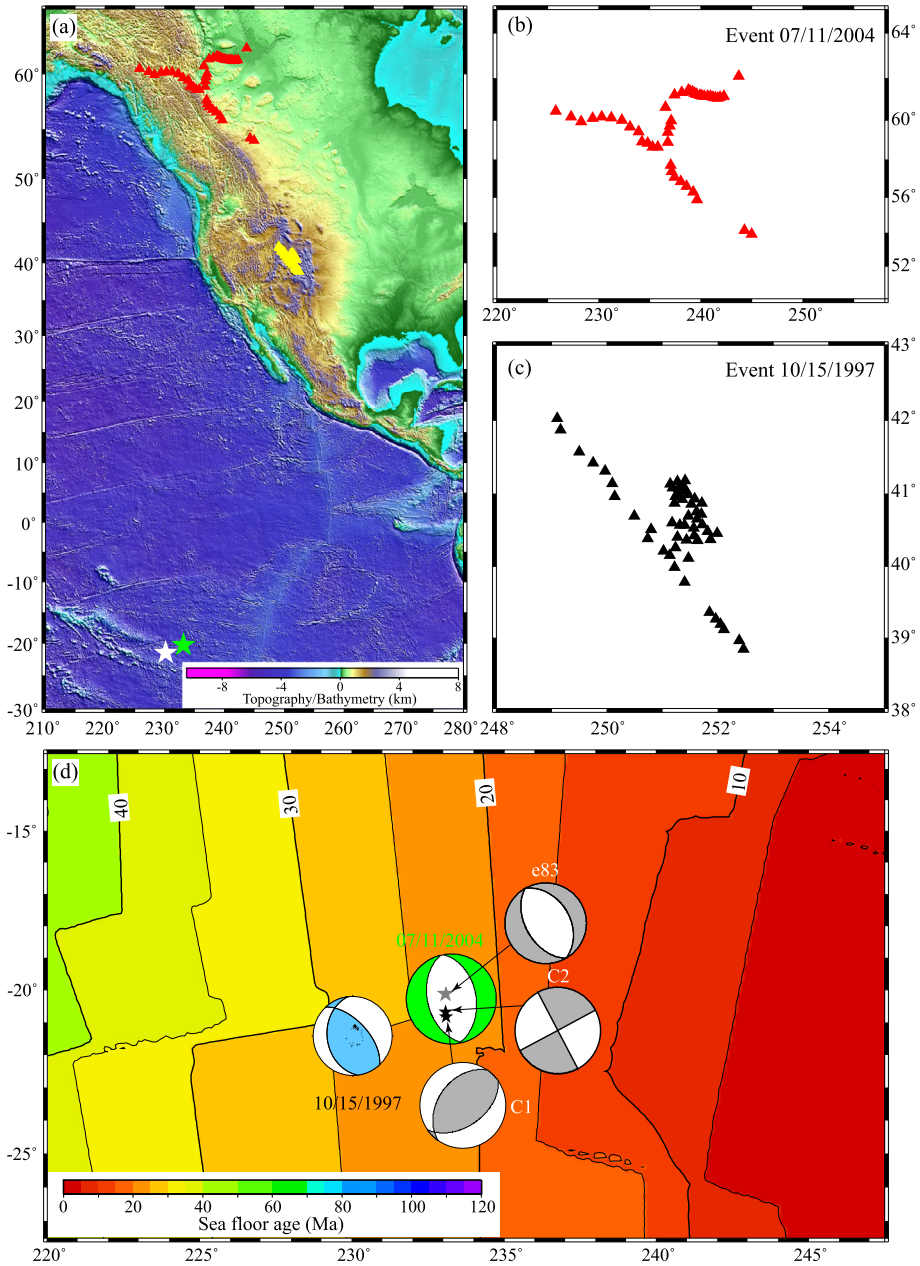

Fig. 4. Maps showing the geographic locations of the two oceanic earthquakes (white and green stars in (a)), the broadband stations used for locating the 07/11/2004 (red triangles in both (a) and (b)) and 10/15/1997 events (yellow triangles in (a) and black triangles in (c)), as well as the sea floor age around the two events (d). (a) Color contour represents the bathymetry and topography with a scale shown in the lower part of the map. (d) The dots within the shaded area of the 10/15/1997 focal sphere indicate the upward first motion observed at teleseismic stations. C1 and C2 refer to the two earthquakes studied by Okal et al. (1980), and e83 refers to the earthquake investigated by Wiens and Stein (1984).

depth (in the range of 3–5 km with an increment of 0.01 km). During the grid search, we set the Moho boundary at 10 km below sea level, which is indicated as the vertical white lines in Fig. 3. We set the P-wave velocity to be 8.04, 6.30 and 1.50 km/s for the mantle, crust, and seawater, respectively. These values are identical to those used in the forward modeling. For the crustal earthquake, the resulting focal and seafloor depths are 7.04 and 3.99 km (Fig. 3a), respectively. Both are near the true depths, 7.00 and 4.00 km. For the upper mantle earthquake, the resulting focal and sea floor depths are 14.91 and 4.00 km (Fig. 3b), respectively.

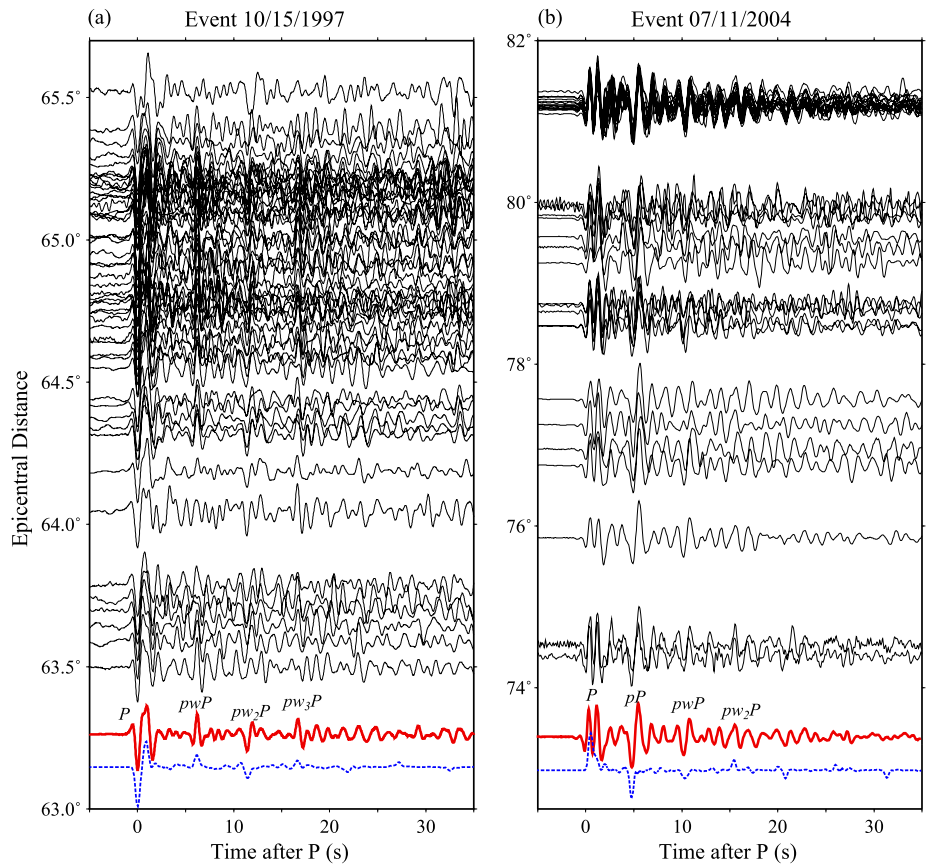

Fig. 5. The observed seismograms of the 10/15/1997 (a, left) and 07/11/2004 earthquakes (b, right) are plotted as a function of epicentral distance. The red and blue traces shown at the bottom respectively are the linear stacks of the observed and synthetic seismograms of each event. (For interpretation of the references to color in this figure, the reader is referred to the web version of this article.)

Table 2
Source parameters of the two events with relocated focal depths.

Origin time		Epicenter		M_w	Depth (km)			Focal mechanism
Date	Time	Lat.	Lon.		PDE	EHB	This study	
10/15/1997	20:23:11.05	−21.468°	−129.856°	5.2	10.0	10.0	6.5 ± 0.2	317/60/70 173/35/120
07/11/2004	23:46:12.48	−20.235°	−126.911°	6.1	12.1	12.9	20.8 ± 0.4	350/44/−87 166/46/−93

The former is near the input value of 15 km while the latter is the exact input value.

3. Application: data and analysis

We avoid the use of earthquakes in the Indian Ocean, at one time regarded as intraplate events, but many of which are now recognized as evidence of deformation in diffuse oceanic plate boundaries (Wiens et al., 1985; Gordon et al., 1990; Royer et al., 1997; Royer and Gordon, 1997; Gordon and Houseman, 2015). Thus, we focus instead on the Pacific plate in regions where we believe the earthquakes are truly intraplate. Okal et al. (1980) investigated the intraplate seismicity of the South-Central Pacific plate using the 15-station French Polynesia Seismic Network for the interval of January 1, 1965 to December 31, 1979. They found that two or more earthquakes with body-wave magnitudes >5.0 occurred in each of three localities, which they termed regions A, B, and C. Herein we focus on region C, located east-southeast of the Tuamotu Archipelago, where Okal et al. (1980) investigated 6 events with $m_b \geq 5.1$. They reported mechanisms for two events, a thrust event with a depth below the seafloor of 5 km and a strike-slip event with a depth less than 5 km. The other events also likely had depths less than 5 km below the seafloor (Okal et al., 1980). In contrast, Wiens and Stein (1984) investigated a nearby 1983 earthquake with a normal faulting mechanism and found a depth of 17 km below the seafloor.

Here we apply the Z–H search to waveform data of two oceanic earthquakes in ∼25 Ma old lithosphere near region C (Fig. 4a). The 10/15/1997 event lies about 300 km southwest of region C and the 07/11/2004 lies just north of region C near the event studied by Wiens and Stein (1984). Details of the origin time, hypocenter, and magnitude of the two events are listed in Table 2. The 07/11/2004 event was recorded by 35 broadband stations installed under the Canadian Northwest Experiment (Fig. 4b) and the 10/15/1997 event was recorded by 53 temporary stations in Colorado deployed by the Deep Probe Experiment (Fig. 4c).

The broadband data are pre-processed first by a deconvolution of instrument response, followed by a convolution of the WWSSN (WorldWide Standardized Seismograph Network) short-period instrument response. The WWSSN short-period data appear to possess the best signal-to-noise ratio for teleseismic P wave records for moderate size earthquakes. The seismograms are subsequently aligned so that the maximum amplitude of the P wave, which is normalized to unity, occurs at time zero. The polarity of the seismogram is also reversed when necessary. The preprocessed data of the two events are shown in Fig. 5a and 5b, respectively. We

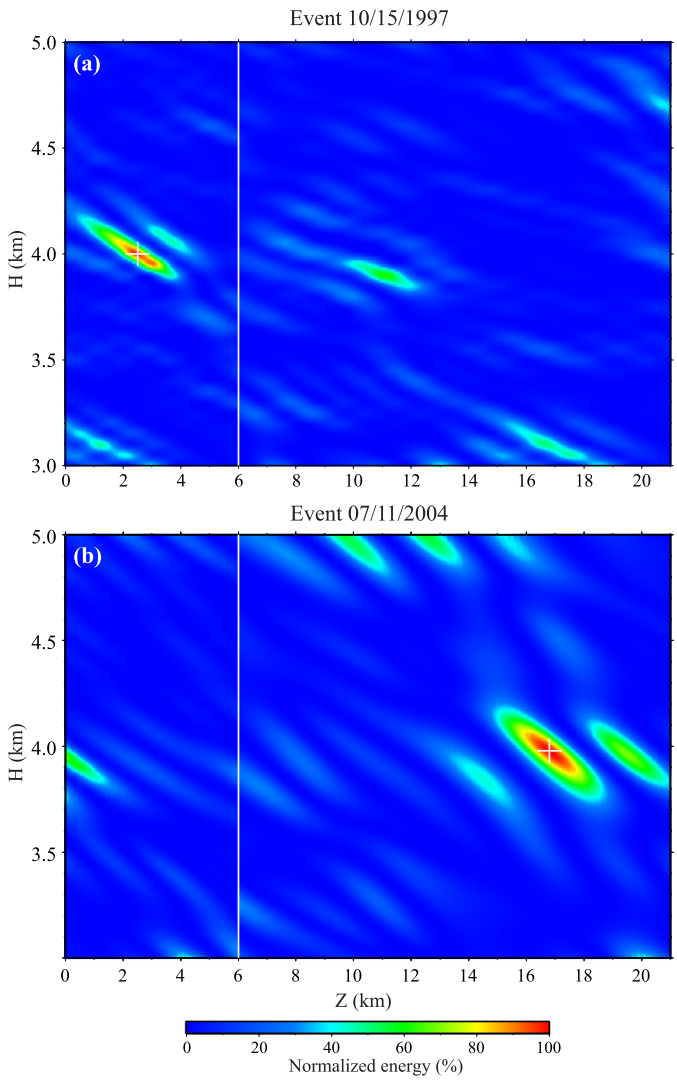

Fig. 6. Same as Fig. 4, but for the two earthquakes occurring in the eastern Pacific. The Z–H search gives optimal (Z, H) grid search results of (2.50, 4.00) km and (16.8, 3.98) km respectively for the 10/15/1997 and 07/11/2004 events, resulting in focal depths of 6.5 and 20.8 km below sea level.

further linearly stack all the seismograms for the Z–H analysis. The stacked seismograms are shown in red in Fig. 5, which clearly show several later arrivals with alternating polarity, indicative of WCRs.

4. Results and discussion

We apply the Z–H grid search to the linearly stacked waveforms of the two events shown in Fig. 5 with search-parameter limits similar to those used in the synthetic data analysis: 0–21 km for Z and 3–5 km for H. The grid spacing is set to 0.01 km for both directions. In computing the relative travel times of the reverberations, we also assume a Moho depth of 10 km beneath sea level, and set the P-wave velocity to be 8.04, 6.30 and 1.50 km/s respectively for the mantle, crust, and seawater.

The Z–H search results of the two events are shown in Fig. 6a, the resulting $(Z,\ H)$ are $(2.50 \pm 0.15,\ 4.00 \pm 0.01)$ and $(16.80 \pm 0.41,\ 3.98 \pm 0.05)$ km respectively for the 10/15/1997 and 07/11/2004 events. The uncertainties shown here are calculated based on a bootstrap method (Efron and Tibshirani, 1986). The estimated water depths are consistent with the depths of ETOPO1 (Amante and Eakins, 2009), which indicates ocean depths of 4.00 and 3.79 km beneath the two epicenters. Thus it is likely that the 10/15/1997 earthquake occurred in oceanic crust, while the 07/11/2004 event ruptured in mantle lithosphere.

The forward modeling of the Z–H analysis depends on the assumed values of crustal velocity (V_c), mantle velocity (V_m), Moho depth (Z_m), and ray parameter or the takeoff angle (θ_c) of the WCRs. We investigated whether errors in these parameters can significantly affect the estimated Z and H by computing reflectivity synthetics with the model listed in Table 1. In the forward modeling of the Z–H analysis, we employ a variety of velocity models in computing the reverberation traveltimes. For each model, we change the value of only one parameter. V_c, V_m, and θ_c are perturbed around their true values by ±5% with an increment of 0.2%, and Z_m is set in the range of 8–12 km with an interval of 0.1 km. Fig. 7 shows the difference between the recovered and input focal depth due to errors in the four parameters. In general, errors in the estimated focal depth Zs associated with uncertainties in the reference velocity model are less than 1 km.

In the schematic synthetic seismogram shown in Fig. 1b, we have ignored the sP depth phase, which is an S-to-P converted phase at the sea floor. In general, the S-to-P transmission coefficient at the sea floor for an upgoing S wave is small (Aki and Richards, 1980). Therefore it is impossible for sP to generate reverberations (spw_nP) inside the water. If there are multiple arrivals after the direct P wave with alternating polarity, then they must be the WCRs resulting from the upgoing P wave (pP). Thus equation (1) is always correct in computing the traveltimes of the multiples even in the presence of a strong sP phase.

In principle, earthquake focal depths can be constrained by careful waveform modeling when the focal mechanism solutions of earthquakes are known (Chu et al., 2009). The focal mechanism solutions of oceanic earthquakes of intermediate size are, however, difficult to obtain due to the lack of local seismic records and to the lower SNR of teleseismic data. The conventional depth-phase method, on the other hand, relies on the robust identification of the depth phases, which is impossible for shallow earthquakes. Our method does not require the full knowledge of earthquake focal mechanisms, and utilizes the travel time of the WCRs, instead of the regular depth phases (pP and sP). Thus we expect it to be more useful for locating shallow oceanic earthquakes of intermediate size when teleseismic array data are available.

The focal depth of the 10/15/1997 and 07/11/2004 events in the PDE catalog respectively are 10.0 and 12.1 km, and the EHB (Engdahl et al., 1998) relocated depths of the two events respectively are 10.0 and 12.9 km. Both suggest that the two earthquakes initiated at roughly the same depth. On the other hand, the two epicenters are ∼335 km apart from each other, and the lithosphere has an age difference of 2 Ma (Fig. 4d). With the PDE focal depth, the difference in focal mechanism of these two earthquakes can only be attributed to the slight age difference or other farfetched explanations. With our relocated focal depth, the difference in focal mechanism can also be related to the depth dependence of the stress field because the 07/11/2004 earthquake occurred at a much greater depth than the 10/15/1997 event.

The global CMT catalog (Dziewonski et al., 1981; Ekstrom et al., 2012) shows that the 07/11/2004 earthquake has a normal faulting mechanism (Fig. 4d), indicating that the oceanic lithosphere is in a stress regime characterized by horizontal deviatoric tension approximately parallel to the age gradient (i.e., perpendicular to the ancient ridge axis). The depth and mechanism are similar to the nearby event analyzed by Wiens and Stein (1984) (Fig. 4d).

The 10/15/1997 Ms 5.3 event was excluded from the global CMT catalog because of its low magnitude. We determine its double-couple focal mechanism using teleseismic data with the CAPjoint software package (Chen et al., 2015) (Table 2, Fig. 4d). Because of its low magnitude (Mw 5.2), there are few shear wave-

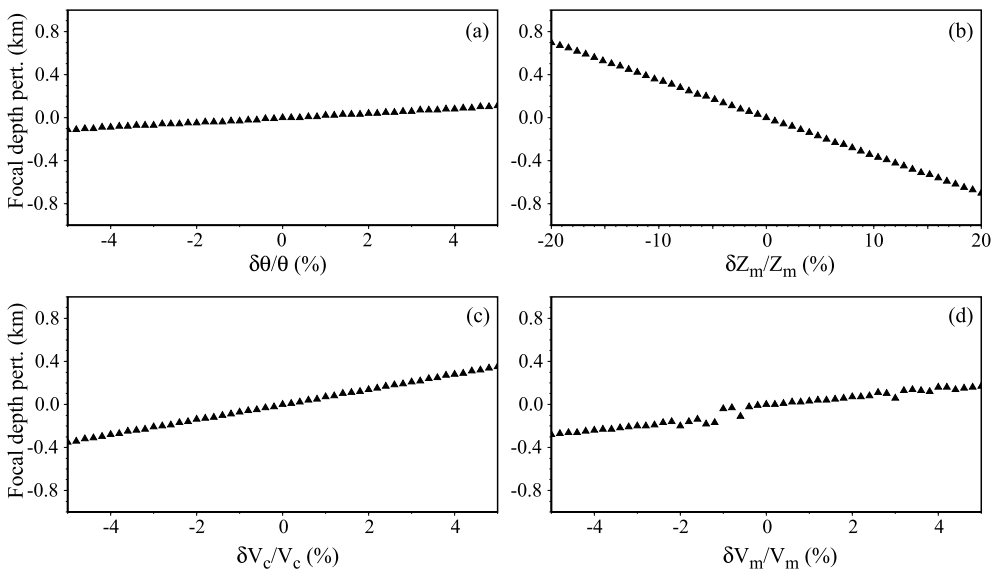

Fig. 7. Robustness analyses of the Z–H grid search method for potential errors in the takeoff angle of the P wave (a), the Moho depth in the reference velocity model (b), crustal (c), and mantle (d) P-wave velocities in the reference model. We allow a perturbation of ±5% in the incident angle and crustal and mantle P-wave velocities, and 20% in Moho depth to use them to recalculate the focal depths (Zs) for a synthetic with a focal depth of 7 km. In general, the resulting errors in the measured focal depth are less than 1 km.

forms that can be used. Therefore we cannot fully constrain the focal mechanism, although it well explains the polarity data of the teleseismic P waves (Fig. 4d). The estimated focal mechanism has a thrust or reverse faulting mechanism (Fig. 4d), which is consistent with the global pattern of oceanic intraplate thrust events being at shallower depths than normal-faulting events, although few events as shallow as this are observed. It is interesting to compare this mechanism with the two determined by Okal et al. (1980) in region C, both of which were also shallow events, one of which was a strike-slip event with a P axis at 107°, and the other of which was a reverse event with a poorly constrained P-axis possibly in a NW–SE direction. Okal et al. (1980) note that most P axes for events in the region tend to be NW–SE. In contrast, the P axis for the 10/15/1997 event is NE–SW. At first, it may seem surprising that the P axis from this event is perpendicular to those from nearby events. According to the shrinking plate hypothesis, however, the upper competent lithosphere should be shrinking in all horizontal directions (Kumar and Gordon, 2009; Kreemer and Gordon, 2014; Mishra and Gordon, submitted for publication). In such a strain field, it is expected that two orthogonal sets of thrust or reverse faults would be present (Houseman and England, 1986; Gordon and Houseman, 2015). The 10/15/1997 event may sample the set of thrust faults perpendicular to those studied by Okal et al. (1980).

5. Conclusions

We develop a new technique for the accurate determination of the focal depth of oceanic earthquakes using water column reverberations recorded at teleseismic distances. Numerical tests suggest that the method is insensitive to the reference velocity model and can robustly recover the input focal depth of various types of earthquakes occurring at different depths inside oceanic lithosphere with an uncertainty less than 1 km. We apply this technique to the teleseismic records of two earthquakes that occurred east-southeast of the Tuamotu Archipelago on 10/15/1997 and 07/11/2004 with a PDE focal depth of ∼10 and ∼12 km, respectively. The estimated focal depths of the two events are 6.5 and 20.8 km below sea level, indicating that they occurred respectively in the oceanic crust and uppermost mantle. The shallow and deep events exhibit a thrust and normal faulting mechanism, respectively, which is consistent with a depth varying stress field predicted from lithospheric cooling models. Moreover, our new thrust mechanism together with prior published mechanisms suggests that the crust in this region is being shortened in two perpendicular horizontal directions. In any event, the Z–H grid search method offers greater precision and accuracy than most cases when the water reverberations are not used.

Acknowledgements

We thank IRIS for providing the data used in this study and Drs. S. Grand at UT Austin and A. Levander at Rice for helpful discussion. We also thank two anonymous reviewers for their constructive comments and suggestions, which significantly improved the quality of this paper. J.H. is supported by the NSFC grants 41104069 and 41274124, as well as the NBRP (National Basic Research Program) 973 projects 2014CB239006 and 2011CB202402, F.N. is supported by NSF grant 1251667. R.G.G. was supported by NSF Grants OCE-0928961 and OCE-1131638.

References

Aki, K., Richards, P.G., 1980. Quantitative Seismology: Theory and Methods. W.H. Freeman, New York. 932 pp.

Amante, C., Eakins, B.W., 2009. ETOPO1 1 arc-minute global relief model: procedures, data sources and analysis. NOAA Technical Memorandum NESDIS NGDC-24. National Geophysical Data Center, NOAA.

Bergman, E.A., Solomon, S.C., 1980. Oceanic intraplate earthquakes: implications for local and regional intraplate stress. J. Geophys. Res. 85, 5389–5410.

Bergman, E.A., Solomon, S.C., 1984. Source mechanisms of earthquakes near mid-ocean ridges from body waveform inversion: implications for the early evolution of oceanic lithosphere. J. Geophys. Res. 89, 11415–11441.

Bergman, E.A., Solomon, S.C., 1988. Transform fault earthquakes in the north Atlantic: source mechanisms and depth of faulting. J. Geophys. Res. 93, 9027–9057.

Chen, W.W., Ni, S.D., Kanamori, H., Wei, S., Jia, Z., Zhu, L., 2015. CAP joint, a computer software package for joint inversion of moderate earthquake source parameters with local and teleseismic waveforms. Seismol. Res. Lett. 86, 432–441.

Chu, R., Zhu, L., Helmberger, D.V., 2009. Determination of earthquake focal depths and source time functions in Central Asia using teleseismic P waveforms. Geophys. Res. Lett. 36, L17317. http://dx.doi.org/10.1029/2009GL039494.

Dziewonski, A.M., Chou, T.-A., Woodhouse, J.H., 1981. Determination of earthquake source parameters from waveform data for studies of global and regional seismicity. J. Geophys. Res. 86, 2825–2852. http://dx.doi.org/10.1029/JB086iB04p02825.

Efron, B., Tibshirani, R., 1986. Bootstrap methods for standard errors, confidence intervals, and other measures of statistical accuracy. Stat. Sci. 1, 54–75.
Ekström, G., Nettles, M., Dziewonski, A.M., 2012. The global CMT project 2004–2010: centroid-moment tensors for 13,017 earthquakes. Phys. Earth Planet. Inter. 200–201, 1–9. http://dx.doi.org/10.1016/j.pepi.2012.04.002.
Engdahl, E.R., van der Hilst, R., Buland, R., 1998. Global teleseismic earthquake relocation with improved travel times and procedures for depth determination. Bull. Seismol. Soc. Am. 88, 722–743.
Engeln, J.F., Wiens, D., Stein, S., 1986. Mechanisms and depths of Atlantic transform fault earthquakes. J. Geophys. Res. 91, 548–577.
Gordon, R.G., DeMets, C., Argus, D.F., 1990. Kinematic constraints on distributed lithospheric deformation in the equatorial Indian Ocean from present motion between the Australian and Indian plates. Tectonics 9, 409–422.
Gordon, R.G., Houseman, G.A., 2015. Deformation of Indian Ocean lithosphere: evidence for a highly nonlinear rheological law. J. Geophys. Res. 120, 4434–4449. http://dx.doi.org/10.1002/2015JB011993.
Heyburn, R., Browers, D., 2008. Earthquake depth estimation using the F trace and associated probability. Bull. Seismol. Soc. Am. 98, 18–35.
Houseman, G., England, P., 1986. Finite strain calculations of continental deformation: 1. Methods and general results for convergent zones. J. Geophys. Res. 91, 3651–3663.
Huang, P.Y., Solomon, S.C., 1988. Centroid depths of mid-ocean ridge earthquakes: dependence on spreading rate. J. Geophys. Res. 93, 13445–13477.
Kennett, B.L.N., Engdahl, E.R., 1991. Traveltimes for global earthquake location and phase identification. Geophys. J. Int. 105, 429–465. http://dx.doi.org/10.1111/j.1365-246X.1991.tb06724.x.
Key, F.A., 1968. Some observations and analyses of signal generated noise. Geophys. J. R. Astron. Soc. 15, 377–392.
Kreemer, C., Gordon, R.G., 2014. Pacific plate deformation from horizontal thermal contraction. Geology 42, 847–850. http://dx.doi.org/10.1130/G35874.1.
Kumar, R.R., Gordon, R.G., 2009. Horizontal thermal contraction of oceanic lithosphere: the ultimate limit to the rigid plate approximation. J. Geophys. Res. 114, B01403. http://dx.doi.org/10.1029/2007JB005473.
McKenzie, D., Jackson, J., Priestley, K., 2005. Thermal structure of oceanic and continental lithosphere. Earth Planet. Sci. Lett. 233, 337–349.
Mendiguren, J.A., 1971. Focal mechanism of a shock in the middle of the Nazca plate. J. Geophys. Res. 76, 3861–3879.
Mishra, J.K., Gordon, R.G., submitted for publication. Tests of the rigid plate and shrinking plate hypotheses. Tectonics.
Okal, E.A., Talandier, J., Sverdrup, K.A., Jordan, T.H., 1980. Seismicity and tectonic stress in the South-Central Pacific. J. Geophys. Res. 85, 6479–6495.
Parmentier, E.M., Haxby, W.F., 1986. Thermal stresses in the oceanic lithosphere: evidence from geoid anomalies at fracture zones. J. Geophys. Res. 91, 7193–7204.
Royer, J.-Y., Gordon, R.G., 1997. The motion and boundary between the Capricorn and Australian Plates. Science 277, 1268–1274.
Royer, J.-Y., Gordon, R.G., DeMets, C., Vogt, P.R., 1997. New limits on the motion between India and Australia since chron 5 (11 Ma) and implications for lithospheric deformation in the equatorial Indian Ocean. Geophys. J. Int. 129, 41–74.
Stein, S., Okal, E.A., 1978. Seismicity and tectonics of the Ninetyeast Ridge area: evidence for internal deformation of the Indian plate. J. Geophys. Res. 83, 2233–2245.
Stewart, G.S., Helmberger, D.V., 1981. The Bermuda earthquake of March 24, 1978: a significant oceanic intraplate event. J. Geophys. Res. 86, 7027–7036.
Sykes, L.R., Sbar, M.L., 1974. Focal mechanism solutions of intraplate earthquakes and stresses in the lithosphere. In: Krisjansson, L. (Ed.), Geodynamics of Iceland and the North Atlantic Area. Reidel, Dordrecht, pp. 207–224.
Wang, R.J., 1999. A simple orthonormalization method for stable and efficient computation of Green's functions. Bull. Seismol. Soc. Am. 89, 733–741.
Wessel, P., 1992. Thermal stresses and the bimodal distribution of elastic thickness estimates of the oceanic lithosphere. J. Geophys. Res. 97, 14177–14193.
Wiens, D.A., Stein, S., 1983. Age dependence of oceanic intraplate seismicity and implications for lithospheric evolution. J. Geophys. Res. 88, 6455–6468.
Wiens, D.A., Stein, S., 1984. Intraplate seismicity and stresses in young oceanic lithosphere. J. Geophys. Res. 89, 11442–11464.
Wiens, D.A., DeMets, C., Gordon, R.G., Stein, S., Argus, D., Engeln, J.F., Lundgren, P., Quible, D., Stein, C., Weinstein, S., Woods, D.F., 1985. A diffuse plate boundary model for Indian Ocean tectonics. Geophys. Res. Lett. 12, 429–432.
Zhao, L.S., Helmberger, D.V., 1994. Source estimation from broadband regional seismograms. Bull. Seismol. Soc. Am. 84, 91–104.
Zhu, L., Helmberger, D.V., 1996. Advancement in source estimation techniques using broadband regional seismograms. Bull. Seismol. Soc. Am. 86, 1634–1641.
Zoback, M.L., et al., 1989. Global patterns of tectonic stress. Nature 341, 291–298.